

Inferring ecological interactions from time series data using neural ordinary differential equations fitted by gradient matching

Willem Bonnaffé^{1,2}, Ben Sheldon¹, & Tim Coulson²

1. Edward Grey Institute of Field Ornithology, Department of Zoology, Oxford University, Zoology Research and Administration Building, 11a Mansfield Road, Oxford OX1 3SZ

2. Ecological and Evolutionary Dynamics Lab, Department of Zoology, Oxford University, Zoology Research and Administration Building, 11a Mansfield Road, Oxford OX1 3SZ

Emails: willem.bonnafe@stx.ox.ac.uk; tim.coulson@zoo.ox.ac.uk

Running title: Repeatable interactions and dynamics

Keywords: Artificial Neural Networks; Ecological Dynamics; Ecological interactions; Geber Method; Neural Ordinary Differential Equations; Ordinary Differential Equations; Prey-predator dynamics; Time series analysis; Rotifers; Microcosm;

Specifications: 140 words in abstract; 7071 words in text; 40 references; 5 figures; 1 table

Contact: Willem Bonnaffé, 61 St Giles, Pusey House, St Cross College, Oxford, OX1 3LZ, UK (w.bonnafe@gmail.com)

Statement of authorship: Willem Bonnaffé designed the method, performed the analysis, wrote the manuscript; Ben Sheldon provided input for the manuscript, commented on the manuscript. Tim Coulson led investigations, provided input for the manuscript, commented on the manuscript.

Abstract

Generalisation of dynamical processes across natural systems is difficult because they are complex and hard to observe. The hope is that generalisation may be achieved by adequately modelling the complexity of systems, and observe them in sufficient detail. We investigate this by looking at the consistency of ecological interactions across three replicates of a three-species prey-predator system, well-observed in an artificial environment, using neural ordinary differential equations. We find that dominant interactions are consistent across the replicates, while weaker interactions are not, leading to different dynamical patterns across replicated systems. Our study hence suggests that generalisation of dynamical processes across systems may not be possible, even in simpler systems in ideal monitoring conditions. This is a problem because if we are not able to make generalisations in a simple artificial system, how can we make generalisation in the real world?

1 Introduction

The repeatability of ecological and evolutionary dynamics varies widely across systems and species. Sticklebacks from different lakes in Canada have independently evolved to a similar river morph phenotype (Thompson, Taylor, and Mcphail 1997). In guppies, four replicated populations located in different streams in Trinidad evolved the same low-predation phenotype (Reznick, Bryga, and Endler 1990). Multiple studies in experimental microcosms, particularly in rotifer populations, have shown that population dynamics were broadly repeatable (Yoshida et al. 2003; Yoshida et al. 2007; Becks et al. 2010; Becks et al. 2012; Hiltunen et al. 2013). Overall, this demonstrated that ecological and evolutionary dynamics may be repeatable across different instances of the same system, at least qualitatively. This was a fascinating finding given the complexity of the mechanisms involved and the subtle variations in environmental conditions across the different populations.

These systems hinted at the possibility for identifying global, generalisable, dynamical models. In practice, however, generalising dynamics and dynamical processes (i.e. functional representations describing which and how state variables affect each other and determine system dynamics) across natural systems has proven difficult (Lawton 1999). First, even if the dynamical patterns, and their outcomes, may appear to be conserved across similar systems, they may be underpinned by different processes. For instance, the evolution of the sticklebacks to highly similar river-adapted phenotypes has been shown to be underpinned by radically different genetic alterations (Raeymaekers et al. 2017). Second, it is often unclear whether quantitative differences across replicated systems

21 arise from pure stochasticity (Dallas et al. 2021), observation error (De Meester et al. 2019), or
22 deterministic changes in the dynamical processes. Finally, the complexity of biological processes
23 themselves (Adamson and Morozov 2013), differences in genetic and environmental contexts, may
24 prevent the identification of a suitable dynamical model. For example, Becks and colleagues found
25 that differences in the initial amount of genetic variation in otherwise identical rotifer populations
26 led to subtle changes to the dynamics (Becks et al. 2010). Different access to seed supplies can
27 modify the strength of the interaction between a plant and its herbivore, leading to either stable or
28 oscillatory dynamics (Bonsall, Van Der Meijden, and Crawley 2003). Differences in temperature
29 can alter the ecological interaction structure of entire ecosystems (Shurin et al. 2012; Bonnaffé
30 et al. 2021). Because of this, vital rates are often found to be inconsistent in time (Gross, Ives, and
31 Nordheim 2005; Adamson and Morozov 2013), and space (e.g. Gamelon et al. 2019). Overall, a
32 growing body of evidence shows that generalisation of dynamical processes across similar natural
33 systems often fails (Lawton 1999, e.g. Kendall et al. 2005; Demyanov, Wood, and Kedwards 2006;
34 Ezard, Côté, and Pelletier 2009).

35 So how could repeatable dynamics arise across multiple instances of the same system? We would
36 expect dynamics to be repeatable if the components of the system (e.g. species), as well as interac-
37 tions between components, are conserved. For this, populations should have similar distributions
38 for the traits that underpin these interactions, and should further share the same environmental con-
39 ditions, across instances. While this is unreasonable to expect from a natural system, it may be
40 achievable in an artificial setting. In such a setting, it is possible to understand the structure of

41 the system, to control the environment, and to reduce observation error. So if we fail to identify
42 and generalise dynamical models in natural systems, perhaps we may be able to do so in artificial
43 systems.

44 In spite of this there are few studies that have attempted to characterise the generalisability of
45 dynamics across replicated systems in a laboratory setting. In such a setting, idiosyncrasies in pop-
46 ulation dynamics can arise from (1) variations in ecological interactions and individual processes,
47 as a result of evolution (e.g. Yoshida et al. 2003), or stochasticity (Dallas et al. 2021), (2) variations
48 in initial conditions due to the experimental setting (Yoshida et al. 2003; Becks et al. 2010; De
49 Meester et al. 2019), and (3) the complexity of the system which can lead to large changes in sys-
50 tem dynamics with small changes in the system state and structure (Adamson and Morozov 2013).

51 Two studies, one in aphids and the other in rotifers, found substantial variation in vital rates across
52 replicated populations, by fitting a stage-structured population ODE model to population dynamics
53 time series data (Bruijning, Jongejans, and Turcotte 2019; Rosenbaum et al. 2019). These studies
54 hint that generalisability of population dynamical processes may not be possible because of in-
55 trinsic population structure and evolution, even in virtually identical populations hosted in artificial
56 environments.

57 We identified three gaps in the literature. First, this kind of evidence remains scarce, due in part
58 to the fact that dynamical modelling approaches guided by empirical data are still not widespread
59 (Pontarp, Brännström, and Petchey 2019). Second, most of these studies relied on parametric
60 frameworks, which impose arbitrary pre-determined forms for the dynamical processes at play, so

61 that their model may not capture properly the complexity of the dynamics of these populations (Jost
62 and Ellner 2000; Adamson and Morozov 2013; Bonnaffé, Sheldon, and Coulson 2021). Finally,
63 most studies usually analyse dynamics in single-species systems, but not multi-species systems,
64 such as those with intraguild predation, which are more biologically realistic scenarios (Hiltunen
65 et al. 2013). Further studies are consequently required to investigate the consistency of dynamical
66 processes in simple multi-species and well-observed systems, to conclude about the generalisability
67 of population dynamics across systems.

68 Our aim in this study is to provide an assessment of the repeatability of dynamical processes across
69 different instances of a realistic multi-species system hosted in a well-observed environment. We
70 do this by quantifying the direction, strength, and consistency of interactions in time and across
71 replicates of a three-species microcosm in an experimental setting. We hypothesise that if the
72 system is (1) simple enough, (2) well-observed, (3) in a controlled environment, then dynamical
73 effects/interactions should be broadly consistent in time and across replicates, hence allowing for
74 generalisation of dynamics across systems. We consider three replicates of a three-species system,
75 consisting in a prey (algae), intermediate-predator (flagellate), and top-predator (rotifer). The algae
76 is consumed by the flagellate and rotifer, and the flagellate is consumed by the rotifer. We use
77 three replicated system runs from a study by Hiltunen and colleagues which feature sequential
78 oscillations of the density of the three species (Hiltunen et al. 2013). We analyse the time series
79 with neural ordinary differential equations (Bonnaffé, Sheldon, and Coulson 2021), which allows
80 us to approximate non-parametrically population growth rates, and quantify the direction, strength,

81 and consistency of inter- and intra-specific effects on the growth of each population. We find that
82 the interaction between the rotifer and algae is consistent throughout time and across replicates,
83 while the interaction between the flagellate and the two other species is not. Our study suggests
84 that dynamical processes may sometimes not be consistent and generalisable across systems, even
85 when they are as close to identical as experimentation permits. We discuss these results and hint at
86 the underlying impact of evolution driving differences in these systems.

87 **2 Material and Methods**

88 **2.1 Method overview**

89 We aim to provide a nonparametric method for estimating ecological interactions from time series
90 data of species density. We do this by approximating the dynamics of each species with neural
91 ordinary differential equations (NODEs, Bonnaffé, Sheldon, and Coulson 2021). We then compute
92 ecological interactions as the sensitivity of these dynamics to a change in the respective species
93 densities.

94 **2.2 Neural ordinary differential equation**

95 A NODE is a class of ordinary differential equation (ODE) that is partly or entirely defined as an
96 artificial neural network (ANN). They are useful to infer dynamical processes non-parametrically
97 from time series data (Bonnaffé, Sheldon, and Coulson 2021). We choose NODEs over standard
98 statistical approaches because they offer two advantages. The first is that NODEs approximate

the dynamics of populations non-parametrically. NODEs are therefore not subjected to incorrect model specifications (Jost and Ellner 2000; Adamson and Morozov 2013). This provides a more objective estimation of the inter-dependences between state variables. The second advantage is that it is a dynamical systems approach. So that the approach includes lag effects through interacting state variables, not only direct effects between them.

For the sake of simplicity, we first consider a two-species NODE system:

$$\begin{cases} \frac{dR}{dt} := r_R(R, N, \beta_R)R \\ \frac{dN}{dt} := r_N(R, N, \beta_N)N \end{cases} \quad (1)$$

where dR/dt and dN/dt denote the change in the density of prey ($R \in \mathcal{R}^+$), and predator ($N \in \mathcal{R}^+$), in continuous time. The per-capita growth rates r_R and r_N are non-parametric functions of the density of each species. The shape of the non-parametric functions is controlled by the parameter vectors β_R and β_N . Traditionally, each non-parametric function is defined as an ANN function of the state variables. The most common class of ANN used for NODEs are single layer perceptrons (SLPs):

$$r_N(R, N, \beta_N) := \beta_0 + \sum_{i=1}^I \beta_i f_\sigma(\beta_{i0} + \beta_{i1}R + \beta_{i2}N) \quad (2)$$

which feature a single layer that maps the inputs, here the species densities R and N , to a single output, the per-capita growth rate. The parameter vector β_R and β_N are the weights of the connections in the SLPs. SLPs can be viewed as weighted sums of basis functions f_σ . More details regarding

114 these models can be found in our previous work (Bonnaffé, Sheldon, and Coulson 2021).

115 **2.3 Fitting NODEs by gradient matching**

116 This section describes how to estimate the parameters β of the NODE system given a set of time
117 series. In previous work, we developed a simulation-based approach to fit NODE systems to time
118 series data (Bonnaffé, Sheldon, and Coulson 2021). We would first simulate the NODE system over
119 the entire time series. Then we would compute the error between the predictions of the NODE
120 model and the observations. Finally, we would change the weights of the NODEs to minimise
121 this error. There are two caveats with this approach. The first caveat is that the NODE system
122 has to be simulated over the entire range of the data at every step of the optimisation. This step is
123 computationally expensive to perform. Second, the numerical integration prevents the computation
124 of gradients of the posterior distribution of the model. This prevents the use of efficient gradient
125 descent approaches.

126 Instead, we propose to use a *gradient matching* approach to fit NODEs, which relies on data in-
127 terpolation to approximate states and dynamics. The method we propose here is derived from the
128 *gradient matching* approach that Ellner and colleagues developed to fit ODEs (Ellner, Seifu, and
129 Smith 2002; Wu, Fukuhara, and Takeda 2005). We proceed in three steps, presented graphically in
130 Fig. 1 and detailed in the following sections. First, we interpolate the time series data and dynamics
131 of each species in the system. Second, we train each NODE to satisfy the interpolated dynamics,
132 thereby avoiding the simulation step of the previous method. This amounts to fitting ANNs that

133 take the density of each population as input to the interpolated per-capita growth rates.

134 **Data interpolation**

135 We interpolate the time series and differentiate it with respect to time in order to approximate
 136 the dynamics of the system. We perform the interpolation via non-parametric regression of the
 137 interpolating function on the time series data

$$\epsilon_{N,t}^{(o)}(\Omega_N|N_t) := N_t - \tilde{N}(t, \Omega_N) \quad (3)$$

138 where $\epsilon_{N,t}^{(o)}$, the observation error, is defined as the difference between N_t , the observed value of the
 139 variable at time t , and $\tilde{N}(t, \Omega_N)$, the value predicted by the interpolating function. The interpolating
 140 function is chosen to be a SLP with sinusoid activation functions

$$\tilde{N}(t, \Omega_N) := \exp \left\{ \sum_{i=1}^I \omega_{i0} \sin(\pi(\omega_{i1} + \omega_{i2}t)) \right\} \quad (4)$$

141 where $\tilde{N}(t, \Omega_N)$ is the interpolated state variable, defined as a weighted sum of sinusoid functions of
 142 time. The interpolation parameter vector Ω_N contains the weights ω_{i0} , ω_{i1} , and ω_{i2} which control
 143 the amplitude, shift, and frequency of the oscillations in the time series, respectively. We found
 144 sinusoid activation functions to be most efficient for interpolating population dynamics compared
 145 to other functions (such as sigmoid, hyperbolic). Following this approach we obtain directly an
 146 approximation of the dynamics of the state variable by differentiating the SLP with respect to
 147 time

$$\frac{\partial}{\partial t} \tilde{N}(t, \Omega_N) = \sum_{i=1}^I \omega_{i0} \pi \omega_{i2} \cos(\pi(\omega_{i1} + \omega_{i2}t)) \exp \left\{ \sum_{i=1}^I \omega_{i0} \sin(\pi(\omega_{i1} + \omega_{i2}t)) \right\} \quad (5)$$

148 as well as an analytical expression of the interpolated per-capita growth rate of the populations, by
 149 combining equation (4) and (5)

$$\tilde{r}_N(t, \Omega_N) := \frac{1}{\tilde{N}} \frac{\partial \tilde{N}}{\partial t} = \sum_{i=1}^I \omega_{i0} \pi \omega_{i2} \cos(\pi(\omega_{i1} + \omega_{i2}t)) \quad (6)$$

150 **Fitting NODEs to interpolated data**

151 In a second step, we train the NODE system (1) to satisfy the interpolated dynamics, given the
 152 interpolated state variables. Thanks to the interpolation step, this simply amounts to performing a
 153 non-parametric regression of the NODE-approximated per-capita growth rate (equation 2) on the
 154 interpolated per-capita growth rate (equation 6)

$$\varepsilon_{N,t}^{(p)}(\beta_N | \Omega) := \tilde{r}_N(t, \Omega_N) - r_N(\tilde{R}, \tilde{N}, \beta_N) \quad (7)$$

155 where the process error, $\varepsilon_{N,t}^{(p)}$, is defined as the difference between the interpolated growth rate \tilde{r}_N
 156 and the NODE approximation r_N .

157 **Statistical modelling**

158 Overall, fitting the NODE system (1) comes down to two steps. First, we interpolate the data by
 159 finding the parameter vector Ω that minimises the observation error $\varepsilon^{(o)}$ in equation (3). Second,

we fit the approximated per-capita growth rate by finding the parameter vector β that minimises the process error $\varepsilon^{(p)}$ in equation (7).

We use a Bayesian framework to perform Bayesian regularisation and control for over-fitting (Cawley and Talbot 2007). First, we fit the interpolating functions to the time series data. We assume normal distributions for the observation error, $\varepsilon_i^{(o)} \sim \mathcal{N}(0, \sigma^{(o)})$, and for the prior density of the parameters, $\Omega_j \sim \mathcal{N}(0, \gamma_j)$. For the interpolation, we are only interested in fitting the time series accurately, irrespective of the value of $\sigma^{(o)}$ and γ_j . So we perform inference on the second level, by optimising the marginal posterior distribution. To do this, we use the approach developed by Cawley and Talbot to average out the value of the parameters $\sigma^{(o)}$ and γ_j in the full posterior distribution (Cawley and Talbot 2007), assuming gamma hyperpriors $p(\xi) \propto \frac{1}{\xi} \exp\{-\xi\}$. This yields the following expression for the log marginal posterior density of the parameters

$$\log P(\Omega_N | N_0, N_1, \dots, N_I) \propto -\frac{I}{2} \log \left(1 + \sum_{i=1}^I \left(\varepsilon_{N,i}^{(o)} \right)^2 \right) - \frac{J}{2} \log \left(1 + \sum_{j=1}^J \Omega_j^2 \right) \quad (8)$$

where P denotes the marginal posterior distribution, N_i corresponds to the observed density at time i , I is the total number of time steps in the time series, $\varepsilon_{N,i}^{(o)}$ is the observation error at time step i , J is the total number of parameters. More details on how to derive this expression can be found in a supplementary file (Supplementary A).

Then, we fit the non-parametric approximation of the growth rates to the interpolated growth rate. We assume normal distributions for the observation error, $\varepsilon_i^{(p)} \sim \mathcal{N}(0, \sigma^{(p)})$, and for the prior density of the parameters, $\beta_j \sim \mathcal{N}(0, \delta_j)$. This gives the following expression for the log posterior

178 distribution of the parameters given the interpolations

$$\log p(\beta_N|\Omega) \propto -\frac{1}{2} \sum_{i=1}^I \left(\frac{\varepsilon_{N,i}^{(p)}}{\sigma^{(p)}} \right)^2 - \frac{1}{2} \sum_{j=1}^J \left(\frac{\beta_j}{\delta_j} \right)^2 \quad (9)$$

179 where Ω corresponds to the interpolation parameters of all the variables in the system (here Ω_R and
 180 Ω_N), $\varepsilon_{N,i}^{(p)}$ is the process error at time step i , $\sigma^{(p)}$ is the standard deviation of the likelihood, J is
 181 the total number of parameters, δ_j is the standard deviation of the prior distribution of parameter
 182 β_j .

183 2.4 Inference and uncertainty quantification

184 This allows us to calculate the gradient of the posterior distributions with respect to each param-
 185 eter. We can hence use efficient optimisation algorithms, such as BFGS, to optimise the posterior
 186 distributions.

187 This approach also allows us to control for over-fitting by adjusting the constraint on the param-
 188 eters, which is controlled by the standard deviation of the parameter prior distributions, δ_j . This can
 189 be used to control the degree of non-linearity in the response, but also to eliminate specific variables
 190 from the model by constraining their parameters to be close to zero. We identify the appropriate
 191 degree of constraint δ_j on NODE parameters via cross-validation. We train the NODE model on
 192 the first half of the interpolated data and we predict the remaining half. We repeat this process for
 193 various values of δ_j .

194 Finally, we estimate uncertainty in parameter values through anchor sampling, which produces ap-

195 proximate Bayesian estimates of the posterior distribution of the parameters (Pearce et al. 2018).
 196 The technique is simple in that it requires sampling a parameter vector from the prior distribu-
 197 tions, and then optimising the posterior distribution from this starting point. By repeatedly taking
 198 samples, the sampled distribution approaches the posterior distribution and provides estimates and
 199 error around the quantities that can be derived from the models. The expectation of the quantities
 200 can then be approached by computing the mean of the approximated posterior distributions. The
 201 great strength of this approach is that it is unlikely to get stuck in local maxima and provides a
 202 more robust optimisation of the posterior. In this study, we took 100 posterior samples for each
 203 time series, namely a hundred samples for the interpolation, and another hundred for the fitting
 204 of the NODE. The initial value of the parameters were picked from a random normal distribution
 205 with parameters $\sigma \geq 0.4$, which prevented underfitting the time series. We insured that there was
 206 moderate temporal autocorrelation and normality by visualising the residuals of the models. We
 207 also insured that the results were repeatable by running the entire fitting process a second time. We
 208 did not perform cross validation of results as we were only interested in estimating effects within
 209 the time series considered, rather than predicting future time steps.

210 **2.5 Model analysis**

211 We analyse the shape of the per-capita growth rates to recover the interaction between the three
 212 species in the system. In particular, we look at the effect and contribution of each species to the
 213 dynamics of the other. The effect is computed as the sensitivity (i.e. the gradient) of the per-capita
 214 growth rate of a given species with respect to the density of the other species. The contribution is

215 computed following the Geber method (Hairston et al. 2005), which comes down to multiplying
216 the dynamics of a variable by its effects on the other variables. We further compute the importance
217 of a species in driving the dynamics of another by computing its relative contribution compared to
218 other species at each time step. More details on how to recover these quantities can be found in our
219 previous study (Bonnaffé, Sheldon, and Coulson 2021).

220 **3 Case study**

221 **3.1 System**

222 We consider a three-species laboratory microcosm consisting of an algal prey (*Chlorella autroph-*
223 *ica*), a flagellate intermediate predator (*Oxyrrhis marina*), and a rotifer top predator (*Brachionus*
224 *plicatilis*). The algal prey is consumed by the intermediate and top predator, the top predator also
225 consumes the intermediate predator (Arndt 1993). The dynamics of this system, here the daily
226 change in the density of each species, were recorded in three replicated time series experiments
227 performed by Hiltunen and colleagues (Hiltunen et al. 2013, Fig. 1). The aim of their experiment
228 was to determine which type of population dynamics would arise in a system with two predators
229 competing for the same resource (the algae), where one predator (the rotifer) would also be able to
230 consume its competitor (the flagellate). According to their expectations, they found prey-predator
231 oscillations, where the lag between the density peaks of each species reflected their position in the
232 food web. Namely that the peak of algae preceded the flagellate peak, which itself preceded the
233 rotifer peak.

234 Their microcosms are close to true replicates in that environmental conditions, namely temperature,
235 salinity, and nutrient influx, were maintained constant, and initial conditions, that is the initial
236 density of each species, were shared across all replicates. In spite of that, they still found evidence
237 for algae evolution in some parts of the time series, which resulted in a shift of the dynamics from
238 fast prey-predator cycles to slower oscillations, similar to those documented in previous studies on
239 similar systems (Yoshida et al. 2003; Becks et al. 2010), even in lineages where genetic variation in
240 predator defense traits was eliminated at the start of the experiment. Consequently, the time series
241 that they reported are the ones that did not present evidence of evolution, and therefore displayed
242 purely ecological dynamics.

243 We use their time series because they describe a simple yet biologically realistic ecosystem, and
244 because the quality of the replication of their microcosm reduces as much as possible observational
245 and experimental error, and rules out environmental variation (Hiltunen et al. 2013). We digitised
246 these time series by extracting by hand the coordinates of every points in the referential of the axis
247 of the graph of the original study, and analysed them.

248 **3.2 Model specifications**

249 The aim of the modelling approach is to infer the drivers of the dynamics of each species from
250 the time series data. More specifically, we want to quantify the effect of a change in the density
251 of one species on the dynamics of the other species. In this way we can understand which, and
252 to what extent, species interactions drive population dynamics. To do this we use neural ordi-

253 nary differential equation (NODEs), which is a novel methodology allowing us to infer dynamical
 254 processes non-parametrically from time series data (Bonnaffé, Sheldon, and Coulson 2021). We
 255 choose this methodology over traditional approaches because it offers two advantages. The first
 256 lies in the fact that NODEs approximate the dynamics of populations non-parametrically, and are
 257 therefore not subject to incorrect model specifications (Jost and Ellner 2000; Adamson and Morozov
 258 2013). This is important as it offers an objective estimation of the inter-dependences between
 259 state variables, and hence a reliable assessment of whether a species is contributing to the dynamics
 260 of another. The second advantage is that it is a dynamical systems approach, which means that the
 261 effects are estimated in a dynamically consistent system of ODEs (Bonnaffé, Sheldon, and Coulson
 262 2021). This is useful because it accounts for the dynamical nature of the system, so that it includes
 263 lag effects, not just direct correlations between variables.

264 We define a simple NODE system for the three-species system described previously

$$\begin{aligned}
 \frac{dR}{dt} &= r_R(R, G, B, \beta_R)R \\
 \frac{dG}{dt} &= r_G(R, G, B, \beta_G)G \\
 \frac{dB}{dt} &= r_B(R, G, B, \beta_B)B
 \end{aligned} \tag{10}$$

265 where dR/dt , dG/dt , and dB/dt denote the change in rotifer (R), algae (G), and flagellate (B)
 266 density in continuous time. The per-capita growth rates r_R , r_G , and r_B are non-parametric functions
 267 of the density R , G , B of each species. The shapes of the non-parametric functions are controlled
 268 by the parameter vectors β_R , β_G , and β_B . Fitting the NODE system (1) amounts to finding the

parameter vectors, and thereby the per-capita growth rates, that best describe the changes in density observed in the time series data.

Each non-parametric functions is an artificial neural network (ANN). ANNs are powerful mathematical objects that can be trained to approximate the shape of dynamical processes (Funahashi and Nakamura 1993; Chen and Chen 1993). For the sake of simplicity, we consider the simplest form of an ANN which contains a single hidden layer, namely a single layer perceptron (SLP)

$$r_R = \sum_{i=1}^N \beta_i f_{\sigma} (\beta_{i0} + \beta_{i1}R + \beta_{i2}G + \beta_{i3}B) \quad (11)$$

which takes as input the density of each species R , G , and B , and output the corresponding per-capita growth rate. The parameter vector $\beta_R, \beta_G, \beta_B$, contain the weight of the connections in the ANNs. The SLP can be viewed as a weighted sum of basis functions f_{σ} of the state variables of the system. In this study we consider sigmoid basis functions, as they are commonly used and their capacity to approximate any continuous function is well established theoretically (Funahashi and Nakamura 1993). The number of units in the hidden layer N is chosen to be 10, as this is a commonly used number for systems of that size (e.g. Wu, Fukuhara, and Takeda 2005). More details regarding these models can be found in our previous work (Bonnaiffé, Sheldon, and Coulson 2021).

284 **4 Results**

285 We analyse sequentially the dynamics of each species, focussing on the amount of variation in
286 per-capita growth rates explained by the NODE model, the overall direction, consistency, and im-
287 portance of ecological interactions, and differences across replicates. Results are summarised in
288 Table 1 and described in details for each species in the following section.

289 **Drivers of top predator dynamics**

290 Figure 2 presents the drivers of the dynamics of rotifer. The NODE approximation of the per-capita
291 growth rate fits quite well the interpolated per-capita growth rate across all replicates (Fig. 2, A2
292 B2 and C2, $r^2 > 0.7$, Table 1). The analysis of effects reveals overall a positive effect of algae on
293 rotifer growth in all replicates (Fig. 2, A3, B3, C3, green line). The intermediate predator has a
294 positive effect on rotifer growth in replicates A and C only (Fig. 2, A3, B3, C3, blue line). We find
295 positive intra-specific density-dependence in the first replicate only (Fig. 2, A3, red line). Overall,
296 all effects are consistent throughout the time series. The algae is the dominant driver of rotifer
297 dynamics as it accounts for 55%, 93%, and 74% of the change in per-capita growth rates across the
298 three replicates (Table 1, Fig. 2, A5, B5, C5, green line).

299 **Drivers of the prey dynamics**

300 The per-capita growth rate of the algae is well explained by the NODE approximation (Fig. 3,
301 A2, B2, C2, $r^2 > 0.8$, Table 1). Overall, rotifers have a negative impact on the growth of algae
302 in all replicates (Fig. 3, A3, B3, C3, red line). We find evidence for negative density-dependence

in replicate A and positive density-dependence in replicate B, but not in replicate C (Fig. 3, A3, B3, C3, green line). The intermediate predator has an overall negative effect on Algae only in replicate B (Fig. 3, B3, blue line). The main driver of algae dynamics is the rotifer population, which accounts for 58%, 44%, and 90% of the change in algae per-capita growth rate across the three replicates. Density-dependence, however, plays a role in replicate A and B, with 40% and 24% of total change in growth, respectively (Table 1). The intermediate predator contributes only to algae growth in replicate B, accounting for 32% change in growth (Table 1). Overall, effects are found to be consistent throughout the time series except in replicate B (Fig. 3, B3), where effects vary in complicated ways, leading to a period in the time series where the algae is mostly driven by the intermediate predator and positive density-dependence, and less impacted by the top predator (Fig. 3, B5, from time 3 to 7.5).

Drivers of the intermediate predator dynamics

The per-capita growth rate of the intermediate predator is quite well captured by the NODE approximation (Fig. 4, A2, B2, C2, $r^2 > 0.7$, Table 1). The intermediate predator is mainly negatively affected by the rotifer population (Fig. 4, A3, B3, C3, red line). The algae has a negative effect on flagellate growth in replicate A, and a positive one in replicate B (Fig. 4, A3, B3, green line). The rotifer predator dynamics accounts for 78%, 62%, 91% of the change in the flagellate growth rate, and the algae 20% and 37% in replicate A and B, respectively (Table 1, Fig. 4, A5, B5, C5). Overall, effects are consistent throughout the time series.

5 Discussion

Our ability to generalise dynamical processes and patterns across populations and communities is limited by the complexity of the processes, differences in environments, and incomplete and/or erroneous observations. It remains unclear to what extent generalisation would be possible if we overcame these limitations. We tackle this question by looking at the consistency of dynamical patterns across three replicated runs of a simple three-species community, hosted in identical environmental conditions in the lab. We expected to find consistency in the drivers of population dynamics, both in time and across replicates, and thereby demonstrate that generalisation of dynamical processes may be possible if the system states were well-observed and environmental conditions were known. To verify this expectation we (1) characterised the amount of variation in per-capita growth rates that is explainable deterministically, (2) quantified the direction, strength, and importance of ecological interactions for the growth of each population, and (3) described how these varied in time and across replicates. Our results are summarised in Figure 5. We find that only the effect of algae on rotifer ($G \rightarrow R$), and that of rotifer on algae ($R \rightarrow G$) and flagellate ($R \rightarrow B$) are conserved across the replicates. We find strong variation in the direction and importance of intra-specific density-dependence in rotifer ($R \rightarrow R$) and algae ($G \rightarrow G$) growth across the three replicates. The role played by the intermediate predator in the system was also different in all replicates, in that it only contributed substantially to the dynamics of the algae in replicate B ($B \rightarrow G$), and was either negatively, positively, or not affected by the algae ($G \rightarrow B$). Overall, this shows that the dominant interactions are conserved across replicates, but that minor interactions

342 vary substantially in importance and effect. Furthermore, we find that these dynamical processes
343 are more consistent in time within a system, than across replicates. Our results demonstrate that
344 because of partially generalisable dynamical processes, dynamical patterns may not be generalis-
345 able across systems, even with limited observation error and when environmental conditions and
346 community structure are conserved.

347 Overall, our results are consistent with the biology of the system. The rotifer top-predator is found
348 to have a strong negative impact on the two other species, in spite of variation in prey preference
349 across replicates. This is consistent with previous study which have established the importance
350 of rotifers for top-down control of flagellate and algal populations (Arndt 1993; Hiltunen et al.
351 2013). What is more suprising is the positive intra-specific density-dependence in the growth rate
352 of the rotifer population in replicate A. This implies that the population of rotifer grows more at
353 high density. This might be explained by various biological mechanisms, such as cannibalism
354 (Gilbert 1976), though evidence remains limited in the *Brachionus* genus, or higher mating success
355 at high density (Snell and Garman 1986). Similarly, the algae shows signs of positive intra-specific
356 density-dependence in replicate B, though this effect remains confined to a brief period in the time
357 series. This may be due to a higher chance of evading predators at high-density. This shows that the
358 NODEs approach used here recovers results consistent with existing knowledge, but also identify
359 subtle, more intriguing dynamical processes.

360 What might be the drivers of differences in the dynamical processes across these three replicates?
361 One of the main source of variation in dynamics may be differences in the intrinsic structure of

populations, such as variation in traits influencing intra- and inter-specific interactions which may lead to different dynamics (Yoshida et al. 2003; Yoshida et al. 2007; De Meester et al. 2019; Bruijning, Jongejans, and Turcotte 2019). Differences in the phenotypic structure may be due to unaccounted variation in initial conditions (Becks et al. 2010), or variation that developed throughout time as a result of evolution (e.g. Yoshida et al. 2003; Yoshida et al. 2007). In particular, the algae in this system is prone to evolve a predator defence behaviour, by forming clumps, which reduce predation risk (Yoshida et al. 2003; Hiltunen et al. 2013). In their original paper, the authors limited the initial genetic diversity in the algae and focussed on replicates which did not display evidence of evolution, in an attempt to limit the impact of initial variation in phenotypic structure, and of evolution, on the dynamics (Hiltunen et al. 2013). In spite of that, evolution may not be eliminated completely, thus variation in traits governing the interactions between the species in the system may still have developed during the experiment, and led to changes in the dynamical processes across replicates. This would further be consistent with results from Yoshida and colleagues, who showed that evolution of prey defense could lead to ecological dynamics inconsistent with the known trophic interactions (Yoshida et al. 2007). Becks and colleagues also showed that small changes in the initial genotypic diversity could lead to drastically different eco-evolutionary dynamics (Becks et al. 2010). Our study hence reinforces the idea that rapid evolution may prevent generalisation of dynamical processes (Ezard, Côté, and Pelletier 2009; De Meester et al. 2019), and further suggests that this may also be the case in simple systems with limited environmental variation and opportunity for evolution.

382 Alternatively, stochasticity may be a major driver of differences across systems (Dallas et al. 2021).
383 First, stochasticity in initial conditions, arising from the sampling of the communities of each
384 replicate, could introduce differences in the interactions between the three populations. Second,
385 stochasticity in the population dynamics themselves may result in different changes in density lev-
386 els in communities that are otherwise identical. Because our modelling approach is deterministic,
387 it does not directly provide an estimate of the total variation explained by stochasticity. Our mod-
388 elling approach decomposes the variation in the data into observation and process error (Calder et
389 al. 2003). First, the interpolation step introduces residual observation error, namely variation that
390 is not captured by the interpolation. Second, the fitting of the NODE to the interpolation introduces
391 residual process error, which is variation in the observation model that is not explained by the pro-
392 cess modelled by the NODE. Stochasticity in the dynamics could explain the observation and pro-
393 cess residual error (Calder et al. 2003), while stochasticity in initial conditions can only influence
394 differences across replicates. Yet, we find relatively small process and observation error ($> 70\%$
395 of variance explained). So that, the dynamics of the three species are well explained by relatively
396 simple linear deterministic effects between the state variables, which means that though dynamical
397 processes differ across replicates they are reasonably consistent in time within each system. This
398 suggests that stochasticity in dynamics plays a minor role in driving differences in dynamics across
399 replicates, compared to stochasticity in initial conditions. In order to quantify this, we would need
400 to estimate the influence of stochasticity directly. This can be done by modelling explicitly the
401 random distribution of model parameters that underpin the dynamics of populations, which would
402 then inform us about the importance of stochasticity driven by variation at the individual-level (Fox

403 and Kendall 2002). Additionally, we could model stochasticity explicitly in the model with neural
404 stochastic differential equations, which would allow us to separate the amount of change explain-
405 able by the deterministic part of the model, from demographic stochasticity, at each time step (Jia
406 and Benson 2019).

407 Finally, we cannot exclude the potential contribution of unobserved variables that were not moni-
408 tored during the experiment, such as variation in nutrient levels in the chemostat, and which may
409 also lead to differences in the predation and intra-specific interactions across systems (e.g. Bonsall,
410 Van Der Meijden, and Crawley 2003; Fussmann and Blasius 2005; Posey, Alphin, and Cahoon
411 2006).

412 Should we expect limited generalisability of dynamics across systems, even if the complexity of
413 the process is properly captured, environmental conditions known, and the system well-observed?
414 A similar study, that inferred dynamical processes consistency from replicated time series of a
415 simple rotifer system, found substantial variation in vital rates across replicates (Rosenbaum et al.
416 2019), also pointing at a low generalisability of dynamical processes. Yet, the level of replication
417 of the time series of their studies was not as stringent as that of the time series we considered,
418 which leaves room for variability in dynamics to be caused by differences in experimental setup,
419 population history, initial densities. Bruijning and colleagues also found substantial variation in
420 vital rates across clones in a replicated system of aphids, showing that slight phenotypic variations
421 can change the population dynamics, all else being equal (Bruijning, Jongejans, and Turcotte 2019).
422 This phenomenon is likely to be even more important in more complicated systems and in a natural

423 setting where most variables are unobserved, which poses a problem for the generalisation of results
424 across studies and systems (De Meester et al. 2019). How can we expect to generalise dynamics
425 across real systems if we are not able to do so in artificial systems? Overall, our study reinforces
426 the view that general inferences should not be drawn from a single system, and that more efforts
427 are required to distinguish dynamical patterns that are conserved across systems from idiosyncratic
428 ones.

429 Can we trust our models then if they are doomed to provide partly idiosyncratic answers? Our
430 study demonstrates that processes can vary substantially across replicates, so that there may hence
431 not be a single suitable functional form and parametrisation to model them (Lawton 1999). Yet,
432 most of the work to date has involved fitting parametric models to time series data (e.g. Bruijning,
433 Jongejans, and Turcotte 2019; Pontarp, Brännström, and Petchey 2019; Rosenbaum et al. 2019),
434 which provide a very narrow view of the range of possible functions to describe the biological
435 processes at play (Jost and Ellner 2000; Adamson and Morozov 2013). These models are subjective
436 by nature (Jost and Ellner 2000; Adamson and Morozov 2013), and hence not generalisable, so that
437 they greatly reduce our chance at identifying dynamical processes that are idiosyncratic, and those
438 that are transferable.

439 What alternatives do we have then? We propose that NODEs are a suitable framework to study
440 dynamical processes, as they produce inferences that are free of model assumption and facilitate
441 comparison across studies and systems (Bonnaffé, Sheldon, and Coulson 2021). In this sense, our
442 study already provides a potentially more objective depiction of dynamical processes than previous

work with parametric models. Furthermore, in this paper we overcame the practical challenges of implementing NODEs by providing a computationally efficient fitting procedure, relying on time series interpolation, and developed a model selection criterion robust to overfitting. Similar approaches have been proposed in the past, for instance Ellner and colleagues developed a method called gradient matching where they interpolated the data with cubic splines to which they fitted the differential equations (Jost and Ellner 2000; Ellner, Seifu, and Smith 2002). Wu and colleagues also relied on data interpolation of the data with ANNs to fit non-parametric approximations of population vital rates (Wu, Fukuhara, and Takeda 2005). But the approaches were too challenging and cumbersome to be implemented routinely, and were not used to tackle ecological interactions. Overall, our work demonstrates the usefulness of NODEs for inferring ecological interactions from count time series, which could readily be applied to a substantial pool of time series data.

Conclusion

Generalising dynamics across biological systems is hard because of the complexity of the dynamical processes (e.g. ecological interactions), differences in environmental context, and monitoring limitations. It remains unclear whether we could generalise dynamics if we properly modelled complexity, controlled for environmental effects, and observed systems precisely. We addressed this question by looking at the generalisability of dynamical processes across three replicated time series of a three-species system, using the novel framework of NODEs. We found that only the dominant interactions were conserved across the three time series, namely that between the algae and the rotifer, while the role of the intermediate predator varied substantially. Our results hence

463 suggest that generalisation may not seem possible, even in simple system with no environmental
464 variation. Given previous work in this system, the main cause of differences across replicates may
465 be evolution in prey defence traits. We conclude that more work is required, using NODEs, to
466 identify dynamical patterns that are conserved and those that are idiosyncratic across a wider range
467 of systems.

468 **Acknowledgments**

469 We thank warmly the Ecological and Evolutionary Dynamics Lab and Sheldon Lab Group at the
470 department of Zoology for their feedback and support. We thank Ben Sheldon for insightful sug-
471 gestions on early versions of the work. The work was supported by the Oxford-Oxitec scholarship
472 and the NERC DTP.

473 **Data accessibility**

474 All data and code will be made fully available at <https://github.com/WillemBonnafe/NODER/rotifer>.

475 **Statement of authorship**

476 Willem Bonnaffé designed the method, performed the analysis, wrote the manuscript; Tim Coulson
477 led investigations, provided input for the manuscript, commented on the manuscript.

References

- Adamson, M. W. and A. Y. Morozov (2013). “When can we trust our model predictions? Unearthing structural sensitivity in biological systems”. In: *Proceedings of the Royal Society A: Mathematical, Physical and Engineering Sciences* 469.2149, pp. 1–19.
- Arndt, H. (1993). “Rotifers as predators on components of the microbial web (bacteria, heterotrophic flagellates, ciliates) - a review”. In: *Hydrobiologia* 255-256.1, pp. 231–246.
- Becks, L., S. P. Ellner, L. E. Jones, and N. G. J. Hairston (2010). “Reduction of adaptive genetic diversity radically alters eco-evolutionary community dynamics”. In: *Ecology Letters* 13.8, pp. 989–997.
- (2012). “The functional genomics of an eco-evolutionary feedback loop: Linking gene expression, trait evolution, and community dynamics”. In: *Ecology Letters* 15.5, pp. 492–501.
- Bonnaiffé, W., A. Danet, S. Legendre, and E. Edeline (2021). “Comparison of size-structured and species-level trophic networks reveals antagonistic effects of temperature on vertical trophic diversity at the population and species level”. In: *Oikos* 130.8, pp. 1297–1309.
- Bonnaiffé, W., B. C. Sheldon, and T. Coulson (2021). “Neural ordinary differential equations for ecological and evolutionary time series analysis”. In: *Methods in Ecology and Evolution* 2, pp. 1–46.
- Bonsall, M. B., E. Van Der Meijden, and M. J. Crawley (2003). “Contrasting dynamics in the same plant-herbivore interaction”. In: *Proceedings of the National Academy of Sciences of the United States of America* 100.25, pp. 14932–14936.

498 Bruijning, M., E. Jongejans, and M. M. Turcotte (2019). “Demographic responses underlying eco-
 499 evolutionary dynamics as revealed with inverse modelling”. In: *Journal of Animal Ecology* 88.5,
 500 pp. 768–779.

501 Calder, C., M. Lavine, P. Müller, and J. S. Clark (2003). “Incorporating multiple sources of stochas-
 502 ticity into dynamic population models”. In: *Ecology* 84.6, pp. 1395–1402.

503 Cawley, G. C. and N. L. C. Talbot (2007). “Preventing over-fitting during model selection via
 504 bayesian regularisation of the hyper-parameters”. In: *Journal of Machine Learning Research* 8,
 505 pp. 841–861.

506 Chen, T. and H. Chen (1993). “Approximations of Continuous Functionals by Neural Networks
 507 with Application to Dynamic Systems”. In: *IEEE Transactions on Neural Networks* 4.6, pp. 910–
 508 918.

509 Dallas, T., B. A. Melbourne, G. Legault, and A. Hastings (2021). “Initial abundance and stochas-
 510 ticity influence competitive outcome in communities”. In: *Journal of Animal Ecology*, pp. 1–
 511 26.

512 De Meester, L. et al. (2019). “Analysing eco-evolutionary dynamics—The challenging complexity
 513 of the real world”. In: *Functional Ecology* 33.1, pp. 43–59.

514 Demyanov, V., S. N. Wood, and T. J. Kedwards (2006). “Improving ecological impact assessment
 515 by statistical data synthesis using process-based models”. In: *Journal of the Royal Statistical*
 516 *Society. Series C: Applied Statistics* 55.1, pp. 41–62.

517 Ellner, S. P., Y. Seifu, and R. H. Smith (2002). “Fitting Population Dynamic Models to Time-Series
 518 Data by Gradient Matching”. In: *Ecology* 83.8, p. 2256.

519 Ezard, T. H. G., S. D. Côté, and F. Pelletier (2009). “Eco-evolutionary dynamics: Disentangling
520 phenotypic, environmental and population fluctuations”. In: *Philosophical Transactions of the
521 Royal Society B: Biological Sciences* 364.1523, pp. 1491–1498.

522 Fox, G. A. and B. E. Kendall (2002). “Demographic stochasticity and the variance reduction ef-
523 fect”. In: *Ecology* 83.7, pp. 1928–1934.

524 Funahashi, K.-i. and Y. Nakamura (1993). “Approximation of dynamical systems by continuous
525 time recurrent neural networks”. In: *Neural Networks* 6.6, pp. 801–806.

526 Fussmann, G. F. and B. Blasius (2005). “Community response to enrichment is highly sensitive to
527 model structure”. In: *Biology Letters* 1.1, pp. 9–12.

528 Gamelon, M. et al. (2019). “Accounting for interspecific competition and age structure in demo-
529 graphic analyses of density dependence improves predictions of fluctuations in population size”.
530 In: *Ecology Letters* 22.5, pp. 797–806.

531 Gilbert, J. J. (1976). “Selective cannibalism in the rotifer *Asplanchna sieboldi*: Contact recognition
532 of morphotype and clone”. In: *Proceedings of the National Academy of Sciences* 73.9, pp. 3233–
533 3237.

534 Gross, K., A. R. Ives, and E. V. Nordheim (2005). “Estimating fluctuating vital rates from time-
535 series data: A case study of aphid biocontrol”. In: *Ecology* 86.3, pp. 740–752.

536 Hairston, N. G. J., S. P. Ellner, M. A. Geber, T. Yoshida, and J. A. Fox (2005). “Rapid evolution and
537 the convergence of ecological and evolutionary time”. In: *Ecology Letters* 8.10, pp. 1114–1127.

538 Hiltunen, T., L. E. Jones, S. P. Ellner, and N. G. J. Hairston (2013). “Temporal dynamics of a simple
539 community with intraguild predation: an experimental test”. In: *Ecology* 94.4, pp. 773–779.

540 Jia, J. and A. R. Benson (2019). “Neural jump stochastic differential equations”. In: *Advances in*
541 *Neural Information Processing Systems* 32.NeurIPS.

542 Jost, C. and S. P. Ellner (2000). “Testing for predator dependence in predator-prey dynamics: A
543 non-parametric approach”. In: *Proceedings of the Royal Society B: Biological Sciences* 267.1453,
544 pp. 1611–1620.

545 Kendall, B. E. et al. (2005). “Population cycles in the pine looper moth: Dynamical tests of mech-
546 anistic hypotheses”. In: *Ecological Monographs* 75.2, pp. 259–276.

547 Lawton, J. H. (1999). “Are There General Laws in Ecology ?” In: *Oikos* 84.2, pp. 177–192.

548 Pearce, T., F. Leibfried, A. Brintrup, M. Zaki, and A. Neely (2018). “Uncertainty in Neural Net-
549 works: Approximately Bayesian Ensembling”. In: *arXiv*, pp. 1–10.

550 Pontarp, M., Å. Brännström, and O. L. Petchey (2019). “Inferring community assembly processes
551 from macroscopic patterns using dynamic eco-evolutionary models and Approximate Bayesian
552 Computation (ABC)”. In: *Methods in Ecology and Evolution* 10.4, pp. 450–460.

553 Posey, M. H., T. D. Alphin, and L. Cahoon (2006). “Benthic community responses to nutrient en-
554 richment and predator exclusion: Influence of background nutrient concentrations and interactive
555 effects”. In: *Journal of Experimental Marine Biology and Ecology* 330.1, pp. 105–118.

556 Raeymaekers, J. A. M. et al. (2017). “Adaptive and non-adaptive divergence in a common land-
557 scape”. In: *Nature Communications* 8.1, pp. 1–8.

558 Reznick, D. N., H. Bryga, and J. A. Endler (1990). “Experimentally induced life-history evolution
559 in a natural population”. In: *Nature* 346.6282, pp. 357–359.

560 Rosenbaum, B., M. Raatz, G. Weithoff, G. F. Fussmann, and U. Gaedke (2019). “Estimating param-
 561 eters from multiple time series of population dynamics using bayesian inference”. In: *Frontiers*
 562 *in Ecology and Evolution* 6.234, pp. 1–14.

563 Shurin, J. B., J. L. Clasen, H. S. Greig, P. Kratina, and P. L. Thompson (2012). “Warming shifts
 564 top-down and bottom-up control of pond food web structure and function.” In: *Philosophical*
 565 *transactions of the Royal Society of London. Series B, Biological sciences* 367.1605, pp. 3008–
 566 17.

567 Snell, T. W. and B. L. Garman (1986). “Encounter probabilities between male and female rotifers”.
 568 In: *Journal of Experimental Marine Biology and Ecology* 97.3, pp. 221–230.

569 Thompson, C. E., E. B. Taylor, and J. D. Mcphail (1997). “Parallel Evolution of Lake-Stream
 570 Pairs of Threespine Sticklebacks (*Gasterosteus*) Inferred from Mitochondrial DNA Variation”.
 571 In: *Evolution* 51.6, pp. 1955–1965.

572 Wu, J., M. Fukuhara, and T. Takeda (2005). “Parameter estimation of an ecological system by a
 573 neural network with residual minimization training”. In: *Ecological Modelling* 189.3-4, pp. 289–
 574 304.

575 Yoshida, T., S. P. Ellner, L. E. Jones, B. J. M. Bohannan, R. E. Lenski, and N. G. J. Hairston (2007).
 576 “Cryptic population dynamics: Rapid evolution masks trophic interactions”. In: *PLoS Biology*
 577 5.9, pp. 1868–1879.

578 Yoshida, T., L. E. Jones, S. P. Ellner, G. F. Fussmann, and N. G. J. Hairston (2003). “Rapid evo-
 579 lution drives ecological dynamics in a predator – prey system”. In: *Nature* 424.July, pp. 303–
 580 306.

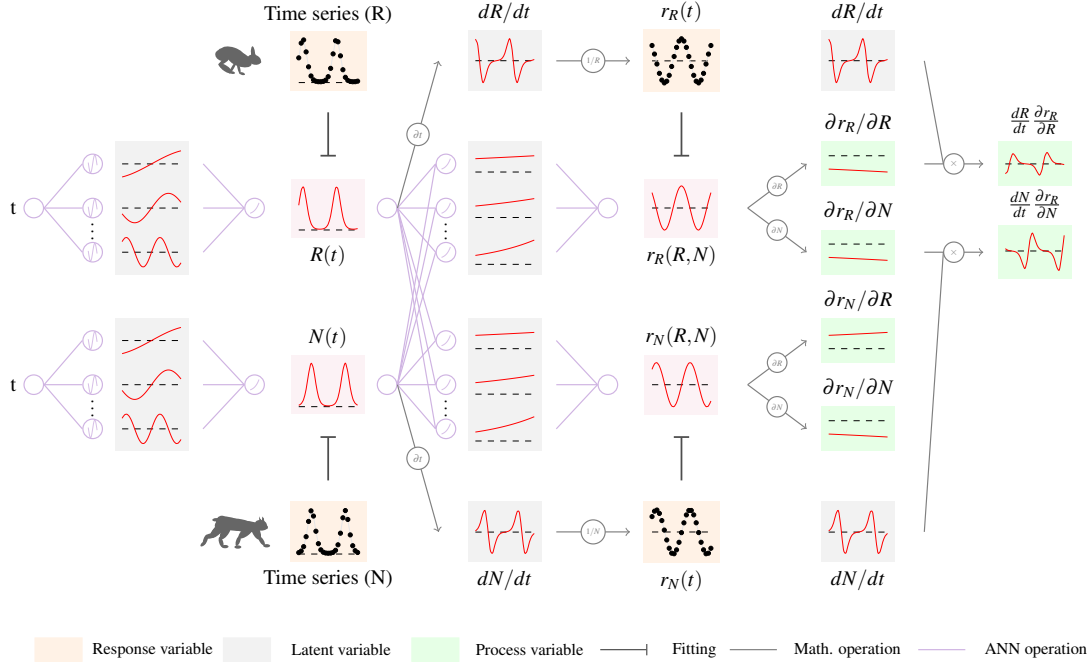


Figure 1: Overview of fitting neural ordinary differential equations by gradient matching

The first step is to compute a continuous time approximation (interpolation) of each state variables (e.g. resource $R(t)$ and predator $N(t)$). To do that we fit an ANN, that takes time as input, to each time series. Dynamics of populations can then be computed by taking the derivative of the ANN with respect to time, dR/dt and dN/dt . This provides an interpolation of the per-capita growth rate of each population, e.g. $r_R(t) = 1/R dR/dt$. In a second step, we approximate non-parametrically the per-capita growth rates with respect to the density of each populations, $r_R = s(R, N)$. To do that we fit an ANN, which takes as input the interpolated variables $R(t)$ and $N(t)$, to the interpolated per-capita growth rates $r_R(t)$ and $r_N(t)$. In a final step, we approximate the ecological interactions, by computing the sensitivity of the per-capita growth rates with respect to the density of each population, e.g. $E : N \rightarrow R = \partial r_R/\partial N$. We also compute the contribution of each species to the dynamics of the other by multiplying the dynamics of each variable with its effect on the growth rates (i.e. the Geber method), e.g. $C : N \rightarrow R = dN/dt \times \partial r_R/\partial N$.

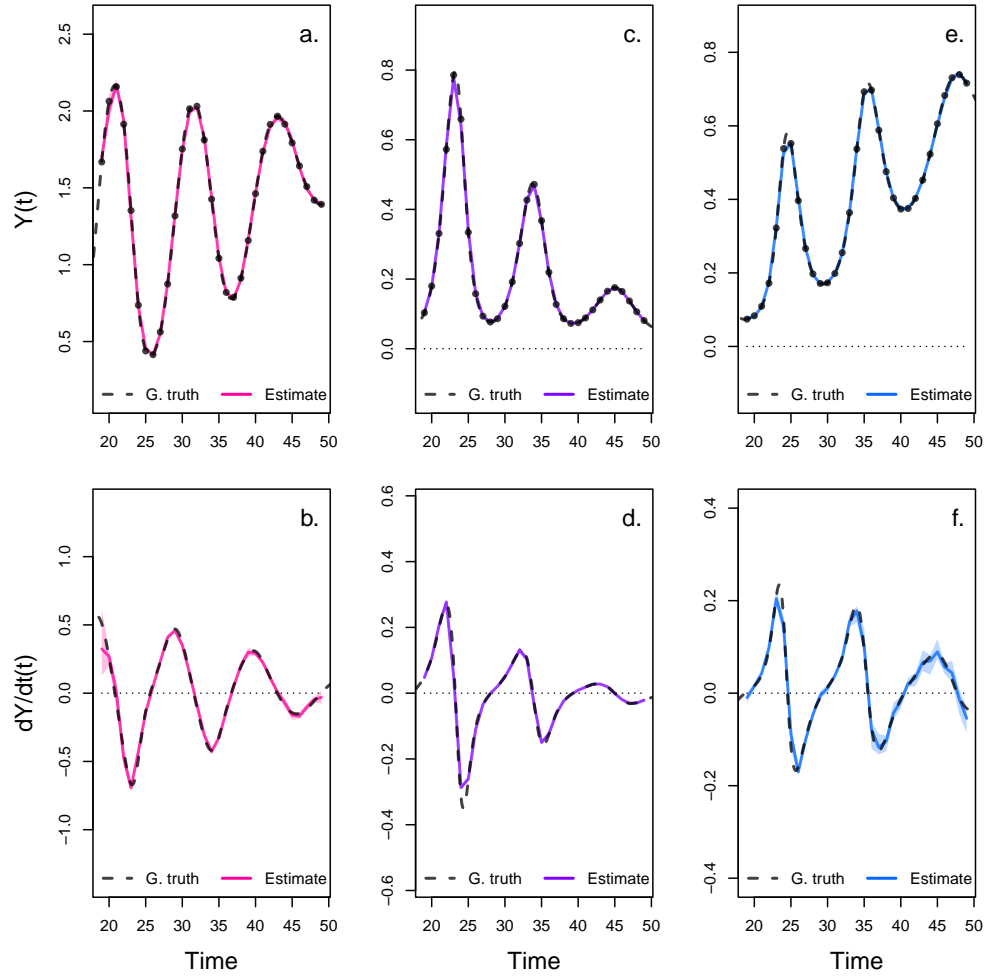


Figure 2: Interpolated density and dynamics of algae, flagellate, and rotifer in the artificial system. This figure corresponds to the first step in the overview figure. It shows the accuracy of the interpolated densities of algae (a.), flagellate (c.), and rotifer (e.). We obtain interpolated densities by fitting observed densities (black dots) with ANNs that take time as input. The observed densities were obtained by sampling a tri-trophic prey-predator ODE model at regular time steps. We then derive interpolated dynamics (b., d., f.) by computing the temporal derivative of the interpolated densities with respect to time. In all graphs, the dashed line represents the ground truth, namely trajectories generated by the ODE model. The solid lines correspond to the interpolations. The shaded area shows the 90% confidence interval, obtained by approximately sampling the marginal posterior distributions.

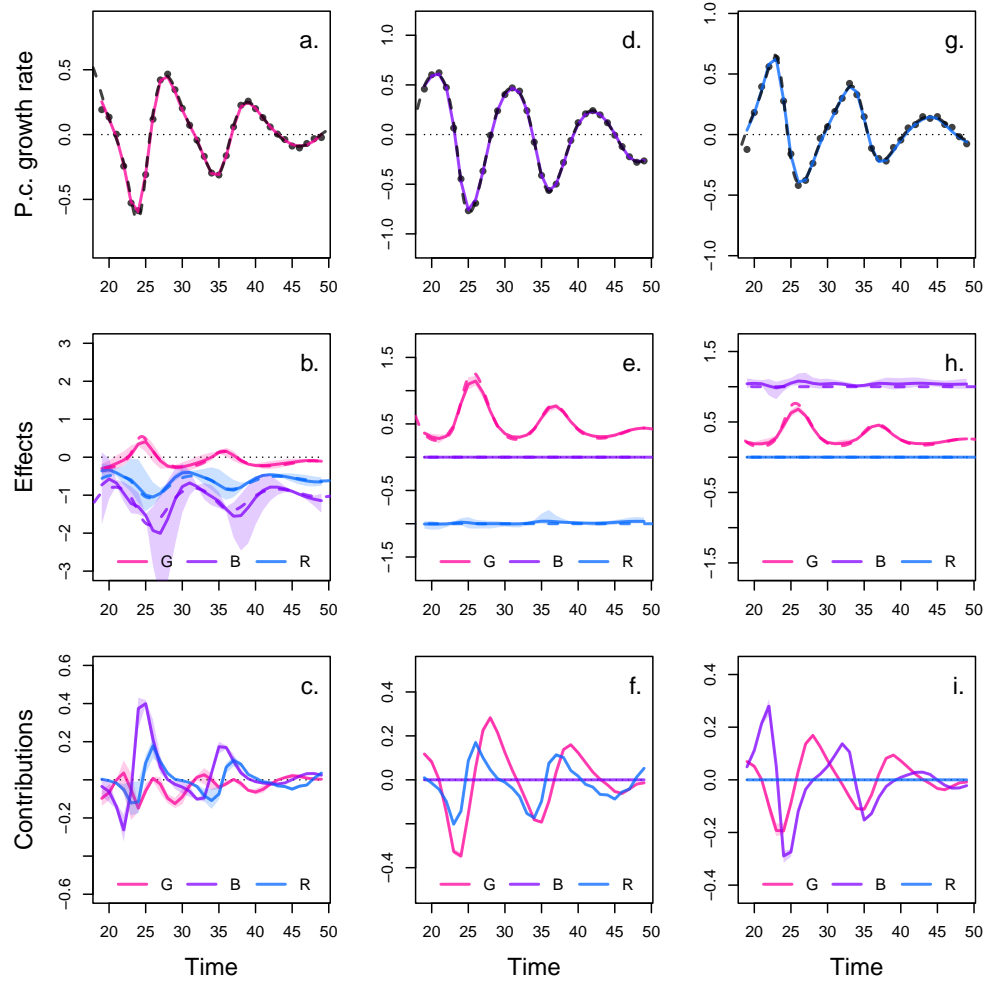


Figure 3: Drivers of dynamics of algae, flagellate, and rotifer in the artificial system. This figure corresponds to the second step in the overview figure. It displays the NODE non-parametric approximations of the per-capita growth rate of algae (a., b., c.), flagellate (d., e., f.), and rotifer (g., h., i.). We obtain the NODE approximations (a., d., g., solid line) by fitting the interpolated per-capita growth rates (black dots) with ANNs that take population densities as input. We then estimate the direction of ecological interactions (effects, b., e., h.) by computing the derivative of the NODE approximations with respect to each density. Finally, we compute the strength of ecological interactions (contributions, c., f., i.) by multiplying the interpolated dynamics of each population (fig. 1, b., d., f.) with its effects. Dashed lines correspond to ground truth, obtained from the original trajectories of the tri-trophic ODE model. The shaded area shows the 90% confidence interval, obtained by approximately sampling the posterior distributions.

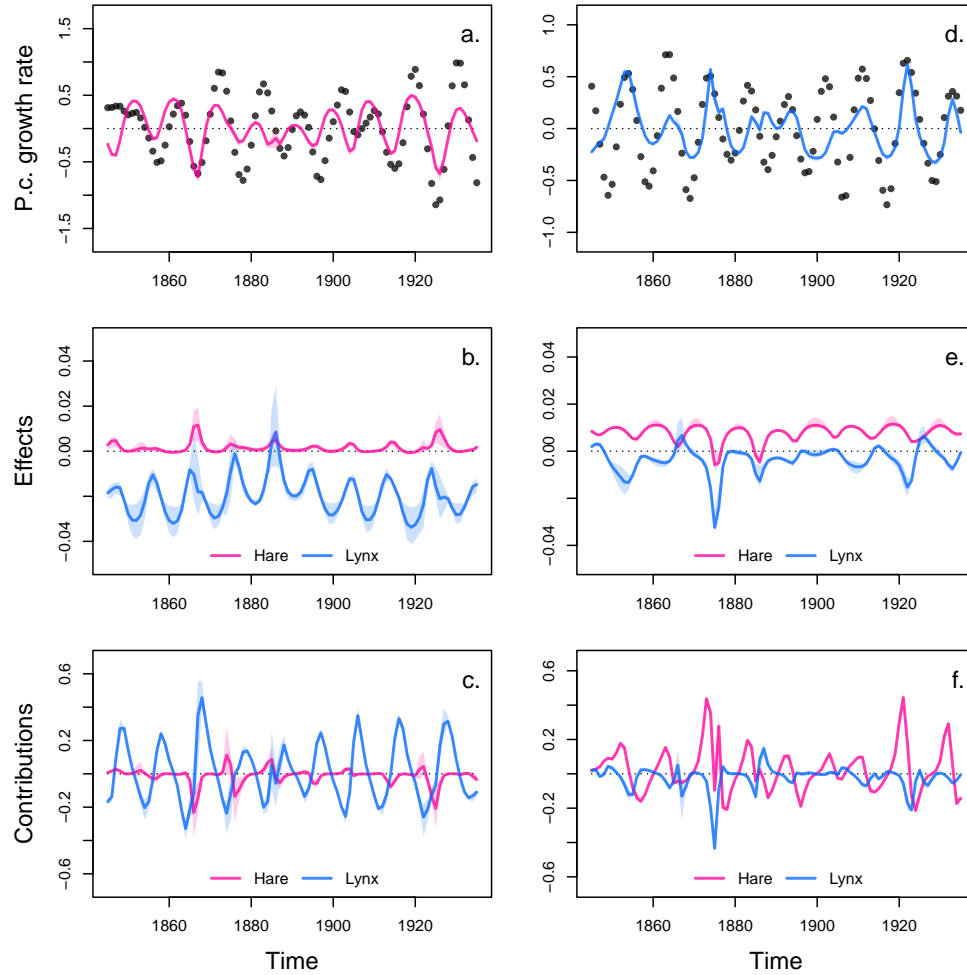


Figure 4: Drivers of dynamics of hare and lynx in the Odum and Barrett pelt count time series. This figure displays the NODE non-parametric approximations of the per-capita growth rate of hare (a., b., c.), and lynx (d., e., f.). We obtain the NODE approximations (a., d., solid line) by fitting the interpolated per-capita growth rates (black dots) with ANNs that take population densities as input. We then estimate the direction of ecological interactions (effects, b., e.) by computing the derivative of the NODE approximations with respect to each density. Finally, we compute the strength of ecological interactions (contributions, c., f.) by multiplying the interpolated dynamics of each population with its effects. The shaded area shows the 90% confidence interval, obtained by approximately sampling the posterior distributions.

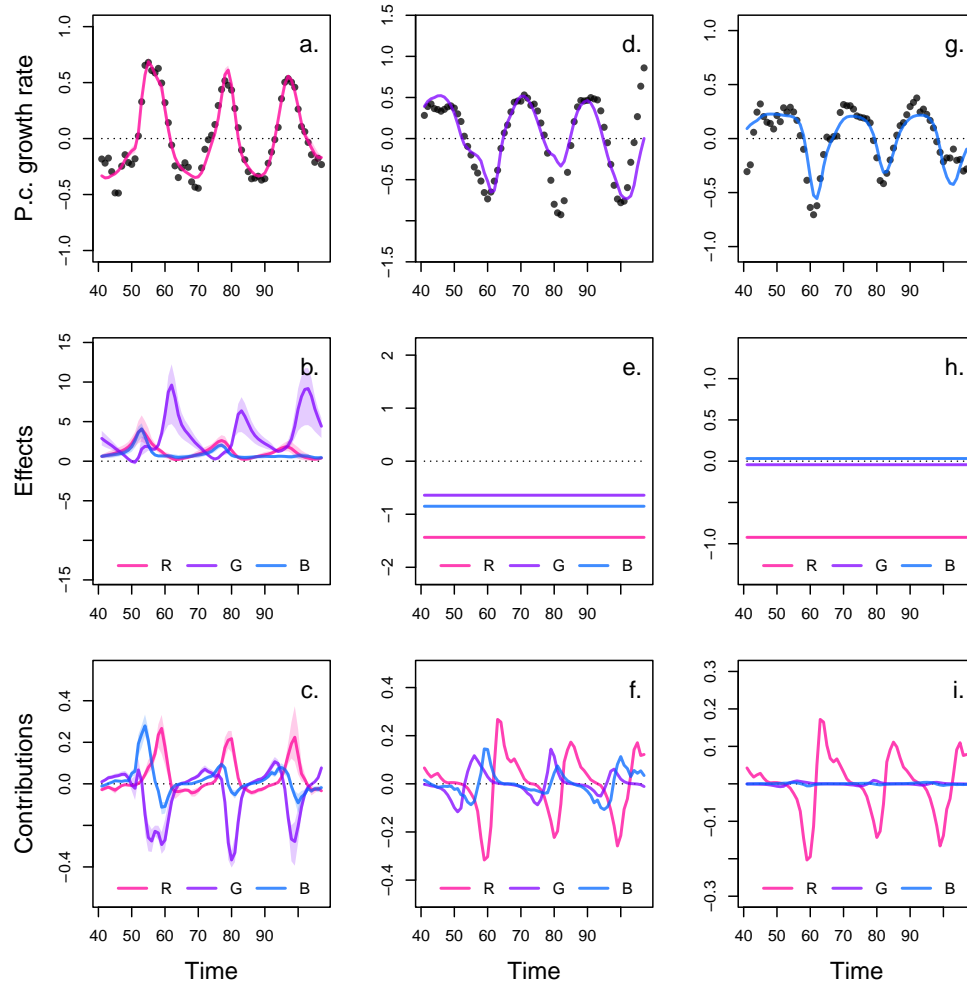


Figure 5: Drivers of dynamics of algae, flagellate, and rotifer in replicate A. This figure displays the NODE non-parametric approximations of the per-capita growth rate of algae (a., b., c.), flagellate (d., e., f.), and rotifer (g., h., i.). We obtain the NODE approximations (a., d., g., solid line) by fitting the interpolated per-capita growth rates (black dots) with ANNs that take population densities as input. We then estimate the direction of ecological interactions (effects, b., e., h.) by computing the derivative of the NODE approximations with respect to each density. Finally, we compute the strength of ecological interactions (contributions, c., f., i.) by multiplying the interpolated dynamics of each population with its effects. The shaded area shows the 90% confidence interval, obtained by approximately sampling the posterior distributions. The replicated time series were obtained by digitising the time series in Hiltunen et al. (2013).

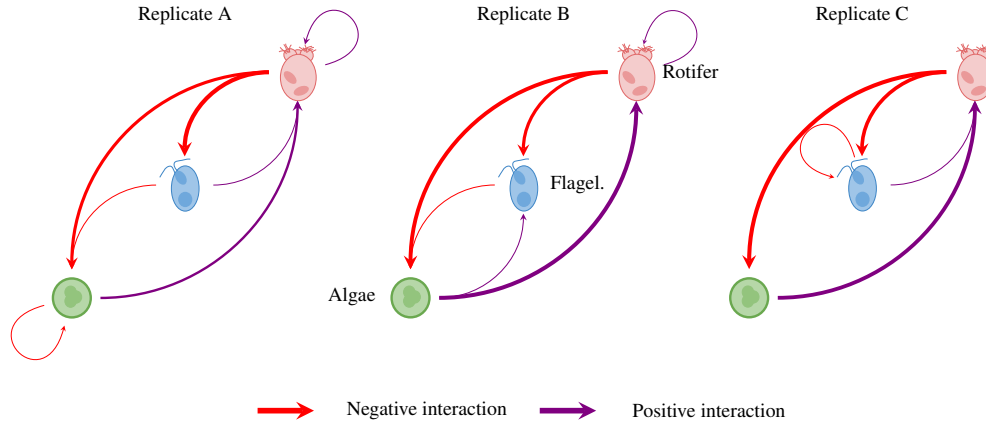


Figure 6: Interaction networks inferred from 3 replicated time series of algae, flagellate, and rotifers. This figure shows the direction and strength of ecological interactions inferred from 3 replicated sets of time series of algae, flagellate, and rotifer, using NODEs fitted by gradient matching. The replicates B and C were analysed in the same way as replicate A (see fig. 5 for details). Red and purple arrows correspond to negative or positive mean effects. We estimated mean effects by averaging effects (i.e. derivative of NODE approximated per-capita growth rates with respect to each population density) across the time series. The width of the arrows is proportional to the relative strength of the ecological interaction. We compute the relative strength as the % of total contributions attributable to either algae, flagellate, or rotifer, obtained from summing the square of contributions of each species throughout the time series. For instance in replicate A, the relative strength of the effect of rotifer on algae is found by summing the square of the red line in fig. 5 f., and computing the % of total contributions that it accounts for. We provide the value of the mean effects and relative strengths in Table 1. The replicated time series were obtained by digitising the time series in Hiltunen et al. (2013).

Table 1: Summary analysis. r^2 corresponds to the r squared of the NODE non-parametric approximation of the pre-capita growth rate compared to the interpolated per-capita growth rate for each of the three species. Mean effects are obtained by averaging the effect of one species on the growth rate of another throughout the time series. The % of total contributions is obtained by summing the square of contributions of one species density to the growth of the other at each time step throughout the time series, then by computing the proportion of total change that it accounts for.

		R	G	B
replicate A				
Mean effects	on R	0.27	0.77	0.97
	on G	-1.17	-0.44	-0.85
	on B	-0.78	0.04	0.03
% of total contributions	to R	0.08	0.48	0.44
	to G	0.75	0.08	0.17
	to B	1	0	0
replicate B				
Mean effects	on R	0.08	0.59	0.22
	on G	-1	0.05	-0.48
	on B	-0.47	0.14	-0.02
% of total contributions	to R	0.02	0.93	0.05
	to G	0.9	0	0.1
	to B	0.9	0.1	0
replicate C				
Mean effects	on R	-0.1	0.45	0.93
	on G	-1.76	-0.13	-0.12
	on B	-0.76	0.01	0.08
% of total contributions	to R	0.01	0.31	0.67
	to G	0.99	0.01	0
	to B	0.99	0	0.01

581 **6 Supplementary**

582 **A Bayesian regularisation**

583 The fitting of the models is performed in a Bayesian framework, considering normal error structure
584 for the residuals, and normal prior density distributions on the parameters

$$p(\theta|\mathcal{D}) \propto p(\mathcal{D}|\theta)p(\theta) \quad (12)$$

585 where θ is the parameter vector of the model, and \mathcal{D} the evidence, namely the data that the model
586 is fitted to. Assuming a normal likelihood for the residuals given the evidence we get

$$p(\mathcal{D}|\theta) = \prod_{i=1}^I \frac{1}{\sqrt{2\pi\sigma^2}} \exp \left\{ -\frac{e_i(\mathcal{D}, \theta)^2}{2\sigma^2} \right\} \quad (13)$$

587 where $e_i(\mathcal{D}, \theta)$ are the residuals of the model given the parameters, and the evidence. In the case of
588 the interpolation, the residuals correspond to the observation error $\varepsilon^{(o)}$ (equation 3). In the case of
589 the NODE approximation, they correspond to the process error $\varepsilon^{(p)}$ (equation 7). I is the number
590 of data points, either observations in the case of the interpolation, or interpolated points in the case
591 of the NODE fitting.

592 The prior probability density functions for the parameters are given by

$$p(\theta) = \prod_{j=1}^J \frac{1}{\sqrt{2\pi\delta_j^2}} \exp \left\{ -\frac{\theta_j^2}{2\delta_j^2} \right\} \quad (14)$$

593 where J is the number of parameters in the models. The parameter δ_j controls the dispersion of the
 594 priors, and thereby the complexity/level of constraint of the model.

595 There is no standard approach for choosing δ . Low values of dispersion may increase constraint
 596 on parameters too drastically, which would lead to underfitting, and result in a reduction of the
 597 variance of parameter estimates and bias mean estimates towards 0. In contrast, too high values of
 598 dispersion may lead to overfitting, by allowing for more complex shapes. To account for this, we
 599 optimise the models on the second-level of inference. This means that we are finding the optimal
 600 value of δ , in addition to optimising the model parameters. We do this by optimising the marginal
 601 posterior density of the parameters, obtained by averaging out δ following a modification of the
 602 approach developed by Cawley and Talbot (Cawley and Talbot 2007). This yields the following
 603 expression for the marginal log posterior density of the parameters

$$\log P(\Omega|\mathcal{D}) \propto -\frac{I}{2} \log \left(1 + \sum_{i=1}^I \left(\varepsilon_i^{(o)} \right)^2 \right) - \frac{J}{2} \log \left(1 + \sum_{j=1}^J \Omega_j^2 \right) \quad (15)$$

$$\log p(\beta|\Omega) \propto -\frac{1}{2} \sum_{i=1}^I \left(\frac{\varepsilon_i^{(p)}}{\sigma} \right)^2 - \frac{1}{2} \sum_{j=1}^J \left(\frac{\beta_j}{\delta_j} \right)^2 \quad (16)$$

604 which amounts to optimising the log of the sum of squared residuals rather than the sum of squared
 605 residuals. $P(\theta|\mathcal{D})$ designates the marginal posterior distribution. More details on how to derive this
 606 expression from equation (8) can be found in a supplementary file (See supplementary A).

607 In this section we describe how to derive the modified model selection criteria developed by Caw-

608 ley and Talbot (Cawley and Talbot 2007). Bayesian regularisation simply amounts to constraining
 609 the values of the parameters in the model to be close to a desired value. Usually, parameters are
 610 constrained by choosing normal priors centered about 0. In this case, the standard deviation of the
 611 normal priors governs the range of values that the parameters can take, and hence constrains more
 612 or less strongly the behaviour of the model (Cawley and Talbot 2007). Performing inference on the
 613 second level means that we are trying to find the appropriate value of the dispersion of the priors,
 614 in other words, the appropriate level of constraint on the model. In practice, choosing the level of
 615 constraint is difficult, Cawley and Talbot hence developed a criterion to perform model selection
 616 on the second level of inference. They proposed to optimise the marginal posterior distribution by
 617 averaging out the dispersion of the priors. With an appropriate choice of prior, the dispersion can
 618 be integrated out, leaving us with a formula for the posterior that only depends on the parameters
 619 of the model,

$$\log P(\theta|\mathcal{D}) \propto -\frac{I}{2} \log \left(\sum_{i=1}^I e_i(\mathcal{D}, \theta)^2 \right) - \frac{J}{2} \log \left(\sum_{j=1}^J \theta_j^2 \right) \quad (17)$$

620 where $P(\theta|\mathcal{D})$ denotes the marginal posterior density, \mathcal{D} denotes the evidence, I and J denote the
 621 number of data points and parameters, respectively, e_i denote the residuals of the model, and θ
 622 denote the parameters of the model. The construction is elegant because it is not sensitive to the
 623 choice of prior hyperparameters, and simple as it amounts to optimising the log of the sum of
 624 squares, rather than the sum of squares (in the case of normal ordinary least square).

625 The issue with this formula is that the marginal posterior density is infinity when the parameters
 626 are 0, which leads to underfitting. In this paper we use a modified criterion, which corrects for that
 627 problem

$$\log P(\theta|\mathcal{D}) \propto -\frac{I}{2} \log \left(1 + \sum_{i=1}^I e_i(\mathcal{D}, \theta)^2 \right) - \frac{J}{2} \log \left(1 + \sum_{j=1}^J \theta_j^2 \right) \quad (18)$$

628 where the marginal posterior density depends only on the residuals of the model when the parame-
 629 ters are equal to 0, and otherwise depends on both the parameters and the residuals. This construc-
 630 tion can be obtained simply by assuming a gamma prior for the parameters $p(\xi) \propto \frac{1}{\xi} \exp\{-\xi\}$,
 631 where ξ is the regularisation parameter, instead of the improper Jeffreys' prior that Cawley and
 632 Talbot used in their original study, namely $p(\xi) \propto \frac{1}{\xi}$. The details of the integration of the posterior
 633 distribution over ξ can be found in Cawley and Talbot's original paper.